East European Journal of Physics. 3. 404-415 (2024)
DOI:10.26565/2312-4334-2024-3-49 ISSN 2312-4334

PERFORMANCE ENHANCEMENT VIA NUMERICAL MODELING AND OPTIMIZATION OF $FASnI_3$ PEROVSKITE SOLAR CELL

Lahcene Kanouni[a], Lamir Saidi[a], Abderrahim Yousfi[b]*, Okba Saidani[b]
[a]*Laboratoire d'Automatique Avancée et d'Analyse des Systèmes (LAAAS), Electronics Department, University of Batna 2, Batna 05000, Algeria*
[b]*ETA Laboratory, Department of electronics, Faculty of sciences and technology, University Mohamed El Bachir El Ibrahimi of Bordj Bou Arréridj-34030, Algeria*
**Corresponding Author: Abderrahim.yousfi@univ-bba.dz; kanouni_lahcene@univ-batna2.dz*
Received May 1, 2024; revised June 10, 2024; accepted June 15, 2024

Perovskite-based solar cells are currently attracting growing interest from researchers and industry alike, thanks to the advantages of this type of solar cell, particularly in terms of manufacturing simplicity and the promising power conversion efficiency, which has recently reached remarkable levels. This paper focuses on numerical simulation to improve the performance of the Formamidinium Tin Iodide ($FASnI_3$) solar cell configuration by using Cerium Dioxide (CeO_2) as ETL and Poly (Triaryl Amine) (PTAA) as HTL. The simulation has been carried out using Solar Cell Capacitance Simulator (SCAPS-1D) tool under the spectrum of AM 1.5 G. An intensive modeling has been realized to improve the output parameters of the suggested configuration based on $FASnI_3$ as absorber. The proposed structure (ITO/CeO_2/$FaSnI_3$/PTAA/Au) achieves a tremendous power conversion efficiency (PCE) of 39.24%, an open-circuit voltage (V_{OC}) of 1.31 V, a short-circuit current density (J_{SC}) of 33.7 mA/cm^2 and a fill factor (FF) of 90.12%.
Keywords: *Solar cell; $FASnI_3$; SCAPS-1D; Optimization; PCE*
PACS: 84.60. Jt

1. INTRODUCTION

Due to the shy efficiency of Si-based photovoltaic solar cells and their high production costs, other materials have been exploited as a solution to the aforementioned drawbacks. Both in research and in commercialization, a certain number of technologies have emerged, such as dye-sensitized solar cells (DSSC), organic photovoltaic cells (OPV), quantum dot solar cells (QDSC), organic-inorganic hybrid solar cells (OIH), and perovskite solar cells (PSC) [1, 2]. According to Best Research-Cell Efficiency Chart published by NREL, the latest perovskite/silicon tandem solar cell, produced by LONGi, achieved a power conversion efficiency of 33.9% [3]. In the other hand, the category of perovskite solar cells, also known as third-generation solar cells, is increasingly attracting researchers due to its promising performance and low costs production.

In the present work, we have focused on organic-inorganic perovskites based on metal halides. Launched in 2009 with a power conversion efficiency of 3.81% [4, 5], perovskite solar cells have improved rapidly, to reach in 2022 a certified PCE of 25.7% [6]. Hybrid organic-inorganic perovskites are expressed as ABX_3, in which A is a monovalent inorganic or organic cation such as methylammonium (MA), formamidinium (FA), or cesium (Cs^+); while B is a divalent cation such as Pb^{2+}, Sn^{2+}, and Ge^{2+}. X is a monovalent anion, such as Cl^-, Br^-, and I^-. In the literature, several combinations have been implemented to exploit the potential of perovskites materials. These choices have been justified in terms of environmental friendliness, production complexity, manufacturing costs and long-term stability, but above all, power conversion efficiency [7, 8]. As an alternative, formamidinium tin iodide ($FASnI_3$, $FA^+ = CH[NH_2]^{2+}$) presents itself as a solution which combines numerous advantages.

In 2023, Shayesteh Imani et al [9] presented a TCO/TiO_2/$CH_3NH_3SnI_3$/HTL/Au structure using different Cu-based as hole transport layer HTLs. They concluded that a CuI-based PCS was an efficient HTL and they achieved with this device a power conversion efficiency of 32.13%, a fill factor of 87.08%, an open-circuit voltage of 1.07 V and a short-circuit current density of 34.35 mA cm^{-2}. Leila Ghalmi et al [10] studied TiO_2/$CH_3NH_3SnI_3$/Cu_2O by adjusting the absorber layer thickness, doping concentration and defect density, and they obtained a remarkable power conversion efficiency of 23.94%.

This work performs a numerical analysis of the proposed device structure (ITO/CeO_2/$FASnI_3$/PTAA). The $FASnI_3$ used as an absorber layer, CeO_2 as electron transport layer (ETL) and PTAA as a hole transport layer (HTL), were used in the simulation using the software Solar Cell Capacitance Simulator SCAPS-1d. We have exploited previous works to conclude on the structure (ITO/CeO_2/$FASnI_3$/PTAA/back contact) and then we will work iteratively to look for the ideal parameters affecting thickness, doping and defect density of all layers. This study will present the effect of varying the above parameters on the output cell parameters such as short-circuit current, open-circuit voltage, fill factor and power conversion efficiency.

2. SIMULATED DEVICE STRUCTURE

The suggested structure in this work is typical to the initial architecture of a PSC cell. The device studied consists of 4 superimposed layers of normal n-i-p order. Figure 1 shows the structure used in this study in the form of ITO/ETL/PVK/HTL/Cathode. The front electrode exposed to sunlight consists of 0.15 µm-thick ITO, used as

Cite as: L. Kanouni, L. Saidi, A. Yousfi, O. Saidani, East Eur. J. Phys. 3, 404 (2024), https://doi.org/10.26565/2312-4334-2024-3-49

a transparent conductive oxide (TCO). The use of CeO_2 as ETL material enables electrons to be collected and efficiently transferred from the absorbing perovskite layer to the front contact material via the electron transfer mechanism, thickness of this layer is 0.015 µm. While PTAA is used as HTL with a thickness of 0.3 µm to collect holes, which transfers the holes from perovskite absorber layer to the back contact. Finally, we use the $FASnI_3$ as absorber material with a thickness of 0.3 µm located as sandwich, between ETL and HTL. The back contact used in the solar cell is Au with a thickness of 0.15µm. The work involves optimizing all the materials used in terms of thickness, doping, temperature, series resistance and work function. The geometrical and electrical input parameters of the current configuration are summarized in Table 1 and 2 for a simulation analysis at temperature of 300 K.

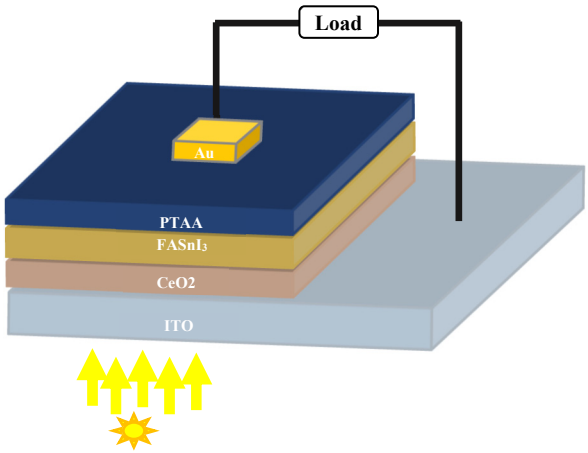

Figure 1. Structure of the designed PSC based on $FASnI_3$.

Table 1. The input parameters in the architecture of simulating device [11-14].

Terms	Parameters	TCO (ITO)	ETL (CeO_2)	PVK ($FASnI_3$)	HTL (PTAA)
Thickness	d (µm)	0.15	0.015	0.3	0.3
Bandgap	E_g (eV)	3.5	3.5	1.3	2.96
Relative Permittivity	ε_r	9	9	8.2	9
Electron affinity	χ (eV)	4	4.6	4.17	2.3
Electron thermal velocity ($cm.s^{-1}$)	v_e	1×10^7	1×10^7	1×10^7	10^7
Hole thermal velocity ($cm.s^{-1}$)	V_h	1×10^7	1×10^7	1×10^7	10^7
Effective DoS at CB.	$N_c(cm^{-3})$	2.2×10^{18}	1×10^{20}	1×10^{18}	1×10^{21}
Effective DoS at VB.	$N_v(cm^{-3})$	1.8×10^{19}	2×10^{21}	1×10^{18}	1×10^{21}
Mob. of electrons	$\mu_n(cm^2/Vs)$	20	10^3	1.6	1
Mob. of holes	$\mu_p(cm^2/Vs)$	10	250	1.6	40
Dop. conc. of the acceptor	$N_a(cm^{-3})$	0	0	3.2×10^{15}	1.5×10^{15}
Dop. conc. of donor	$N_d(cm^{-3})$	1×10^{21}	1×10^{19}	0	0
Defect Density	$N_t(cm^{-3})$	1×10^{15}	1×10^{14}	1×10^{14}	1×10^{14}

Table 2. Parameter of interface defects used in simulations.

Parameters	PTAA/$FASnI_3$	$FASnI_3/CeO_2$
Defect type	Neutral	Neutral
Capture cross section electrons(cm^2)	1×10^{-19}	1×10^{-19}
Capture cross section holes(cm^2)	1×10^{-19}	1×10^{-19}
Energy distributions	Single	Single
Reference for defect energy level	Above the highest EV	Above the highest EV
Energy with respect to reference (eV)	0.6	0.6
Total density (integrated over all energies) (cm^{-2})	1×10^9	1×10^9

3. Mathematical Modelling

The design and simulation of our PSC model were carried out using SCAPS-1D [15, 16]. Burgelman and his team from Gent university have created SCAPS-1D which allows the numerical modeling of photovoltaic components such as solar cells and photodetectors in order to obtain their output parameters like J-V characteristics which results from the multiplication of several parameters such as J_{SC}, V_{OC} and FF. The one-dimensional equation drives semiconductor materials in steady-state conditions [17].

The following equation presents the electric fields and charge density for the *pn* junction [18] :

$$\frac{\partial^2\varphi}{\partial^2 x} = -\frac{\partial E}{\partial x} = -\frac{\rho}{\varepsilon_s} = -\frac{q}{\varepsilon_s}[p - n + N_D^+(x) - N_A^-(x) \pm N_{\text{def}}(x)] \quad (1)$$

The precedent equation contains, the electrostatic potential, the charge, the static relative permittivity, n and p are the electrons and the hole, respectively, while N_A and N_D are the acceptor and donor successively, N_{def} named defect density.

Equation continuity of the electron and hole of the solar cell based perovskite configuration illustrated as follows [19]:

$$\frac{1}{j}\frac{\partial j_p}{\partial x} + R_p(x) - G(x) = 0, \tag{2}$$

$$-\frac{1}{j}\frac{\partial j_n}{\partial x} + R_n(x) - G(x) = 0. \tag{3}$$

The current densities of electron and hole symbolized successively, j_n and j_p, carrier generation rate and recombination rate of electron and hole are respectively, G and $R_{n,p}(x)$.

Synchronously, the current density for both, electrons and holes are illustrated in the following equations[20]

$$j_n = qn\mu_n E(x) - qD_n\frac{\partial n}{\partial x'}, \tag{4}$$

$$j_p = qn\mu_p E(x) + qD_p\frac{\partial p}{\partial x'}. \tag{5}$$

Where, q is the charge, μ_n and μ_p are the electrons and holes mobilities respectively, D_n and D_p are the diffusion coefficients for electrons and holes, respectively.

It should be pointed out that the recombination and generation equations are obtained from the SCAPS-1D simulator.

4. RESULTS AND DISCUSSIONS

The examination of the current solar cell configuration is carried out within the framework of the analysis of photovoltaic and electrical output parameters, which is subdivided into several parts as follows:

4.1 The influence of active layer thickness on the PSC outputs

Due to its impact on photogeneration, charge collection and transport processes, the performance of perovskite solar cells is directly affected by the thickness of the active layer, influencing the optical properties, electrical properties, energy characteristics and morphology of the cells [21]. Figure 2 illustrates the results of simulating the variation of cell parameters as a function of absorber thickness.

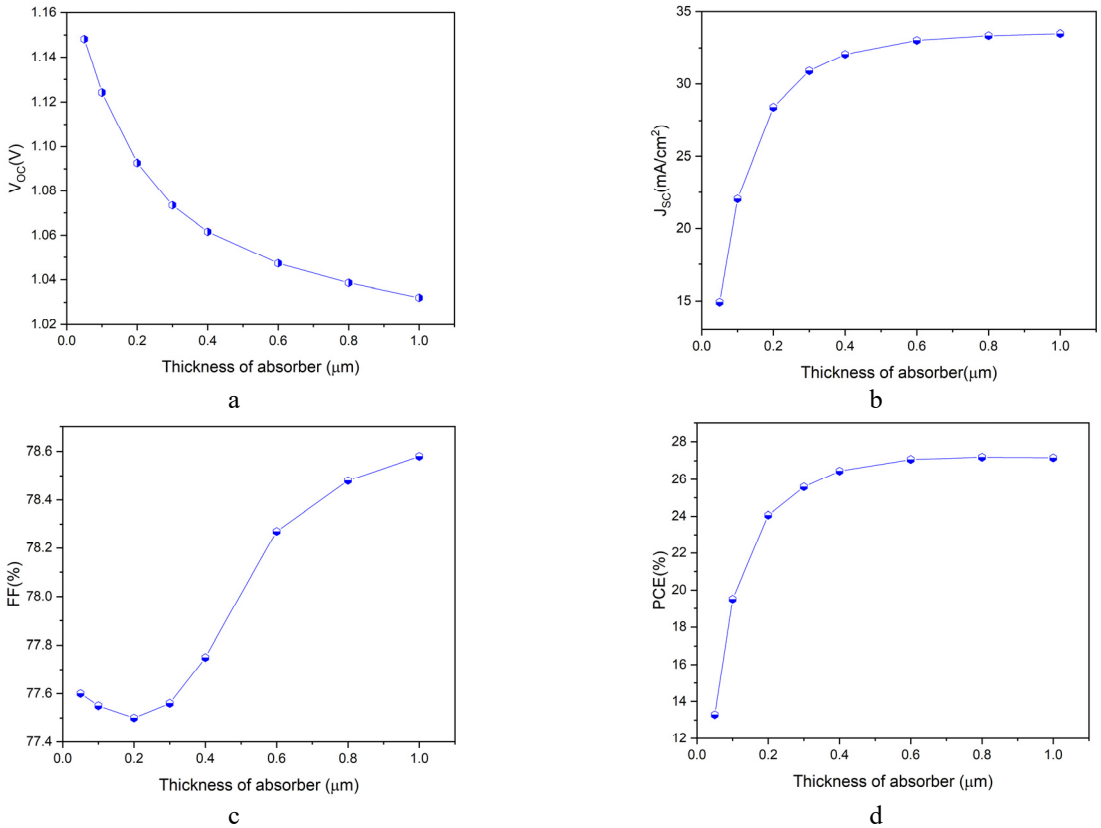

Figure 2. Variation of PV parameters as a function of the absorber layer thickness

We can observe in Fig. 2 (a) the decrease in V_{OC} with the increasing of perovskite material thickness, which varies from 0.1 µm to 1.0 µm, to get respectively the V_{OC} of 1.15 V to 1.034 V because of the wider bandgap of the perovskite

material. In Fig.2 (b), it is clear that the J_{SC} current of the solar cell increases with increasing $FASnI_3$ layer thickness due to increased charge carrier generation and reaches its saturated value of 33.9 mA/cm^2 at 1.0 µm. A similar increase in J_{SC} is reported by Atanu Bag et al. [22]. The fill factor of the current configuration increases from a thickness of 0.2 µm up to the maximum simulated value of 1 µm, as depicted in Fig.2 (c), giving a fill factor of 78.6%. Power conversion efficiency varies up to 0.6 µm, where the curve begins to flatten, leading to PCE saturation at a value of 27.4%, as shown in Fig.2 (d), beyond this, any further increase in thickness produces only marginal and insignificant improvements in PCE.

4.2 Effects of Temperature on PSC output parameters

In general, the operating environment for photovoltaic solar cells is direct sunlight, so the radiation falling on the solar cells raises the temperature. Many authors have reported a significant degradation in cell performance with increasing temperature, which affects all the parameters in the same way [23-25] . As illustrated in Figure 3, the section treats the variation of temperature from 300 K to 380 K to investigate the behavior of the cell in this range. Variation in J_{SC} and V_{OC} are shown in Fig.3 (a) and (b) respectively where the J_{SC}=30.89 mA/cm^2 at the 300 k and the V_{OC}=1.074 V for 300K, whereas at 375K, these two parameters reach their lowest values. As depicted in Fig. 3(c), the relevant FF values are 77.3% and 71% at 300K and 375K respectively. The PCE shows the same negative variation in Fig.3 (d), rising from 25.6% at 300K reaching 21.4% at 375K. We note that the current configuration supports the lower value of temperature cause the all-output parameters works well at 300K and this degraded performance at high temperatures may be due to a number of factors, such as accelerated interfacial recombination, reverse saturation current, bulk defects [26,27].

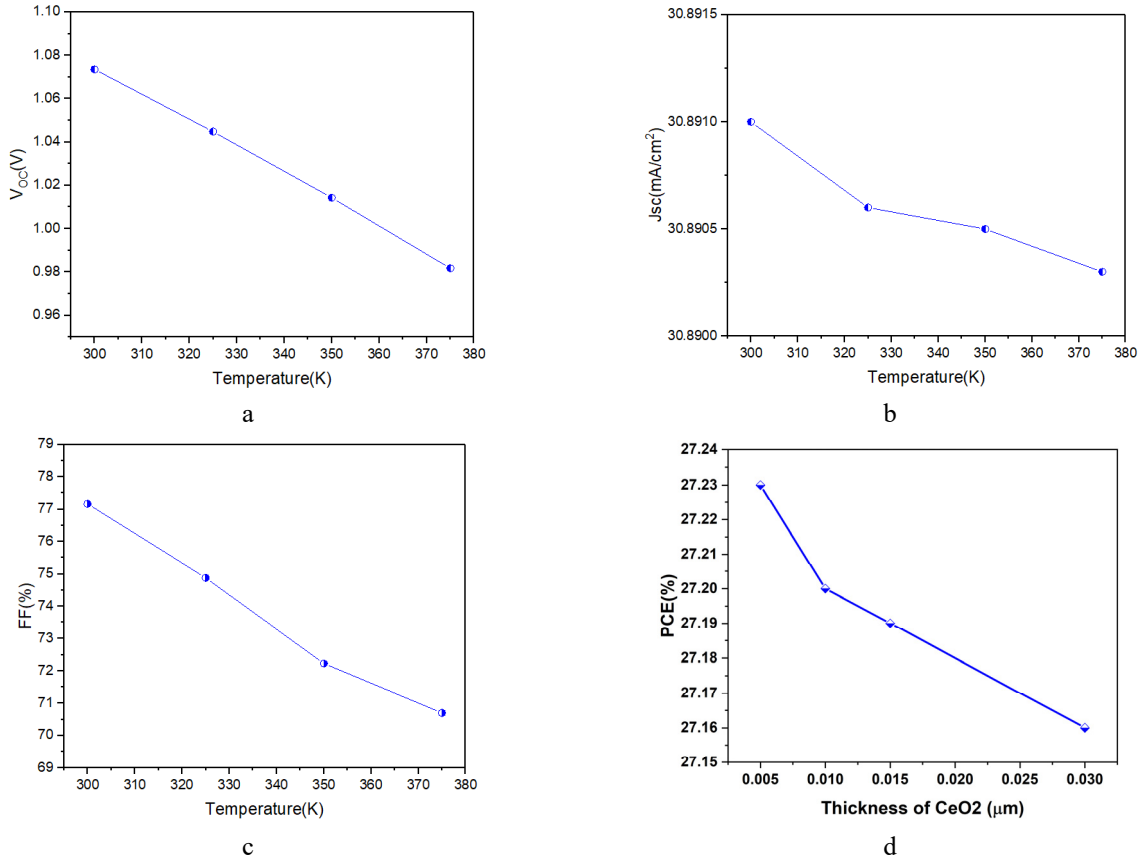

Figure 3. Variation in solar cell parameters as a function of temperature

4.3 The Impact of CeO_2 and PTAA thickness

In line with the previous section on temperature, we have used the default temperature of 300 k for good PVK solar cell performance. The thickness of the ETL and HTL layers can affect the efficiency, stability and reliability of the perovskite solar cell. In this section, the problem of the impact of charges transport layers thickness will be discussed, with Figures 4 and 5 showing V_{OC}, J_{SC}, FF and PCE for different CeO_2 and PTAA thicknesses respectively. These two layers should be as thin as possible to ensure fast electrons and holes transport, low interfacial recombination and low resistance losses, while ETL thickness should have a greater effect on the photovoltaic properties of PSC [28,29].

The variation of performance parameters as a function of CeO_2 thickness is illustrated in figure 4(a-d), in which thickness varies for values ranging from 0.005 µm to 0.03 µm. Simulation results showed that all PSC parameters decreased with increasing CeO_2 ETL layer thickness. Good performance is observed in the 0.005 µm thickness of the ETL used where J_{SC}= 33.375 mA/cm^2, V_{OC}=1.0388 V, FF=78.55% and PCE=27.23%.

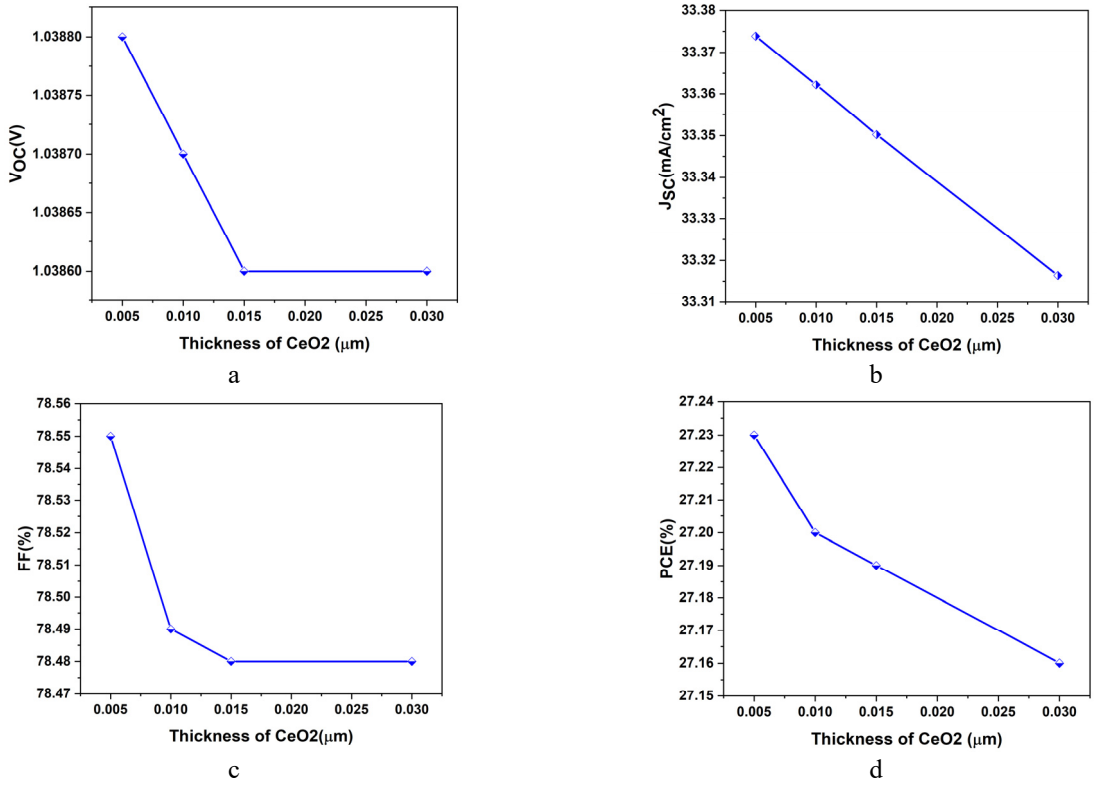

Figure 4. Variation of PV parameters as a function of CeO_2 thickness

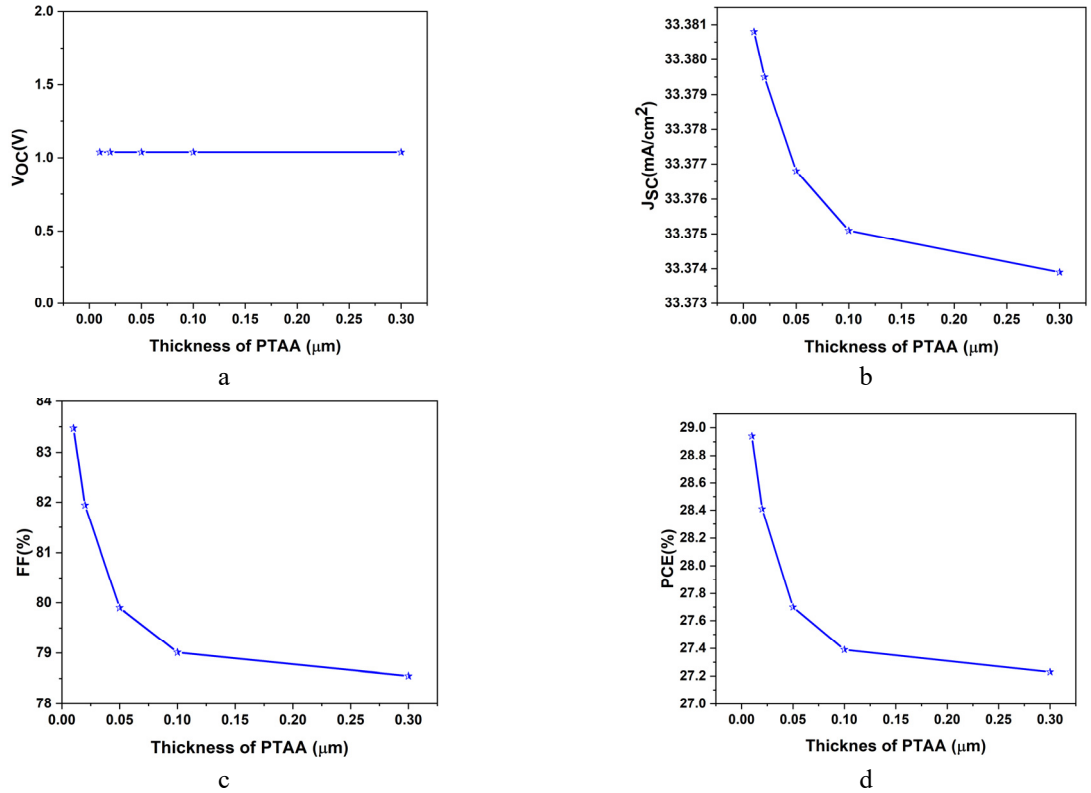

Figure 5. Variation of PV parameters as a function of PTAA thickness

Figure 5(a-d) illustrates the variation of PV parameters as a function of PTAA HTL layer thickness. We note that the highest PCE value obtained is 28.95% for the lowest PTAA thickness value of 0.025 µm. At this point also we had J_{SC}=33.381 mA/cm^2, FF=83.5% and V_{OC} remains fixed at value 1.08 V throughout the thickness range used. Ola Mostafa et al. have developed results similar to those shown in figure 5 [30]. It is evident that thinning the HTL should reduce the distance traveled by the holes to reach the back electrode, thereby reducing the likelihood of them undergoing

recombination [31]. The thicker layer of PTAA therefore acts as an insulator for the holes generated in the absorber by the increased series resistance, resulting in a reduction in J_{sc}, FF and PCE.

4.4 Effect of varying acceptor doping density in the absorber layer

The actual investigation focuses on output parameters as a function of acceptor doping density in the absorber layer. As reported by Md. A. Islam et al [32], doping the absorber layer can reduce the density of trap states and increase carrier lifetime in the cell, thereby increasing V_{OC}. It has also been shown that increasing the doping concentration improves V_{OC} and PCE due to the increase in the built-in electric field, which has the effect of separating charge carriers and reducing charge recombination [33]. To study the impact of acceptor doping density in the absorber layer, the device will be examined by varying the doping concentration from 3.2×E13 cm^{-3} to 3.2×E17 cm^{-3} as shown in figure 6.

As illustrated in Fig. 6 (a, c, d), the variation in output parameters starts to increase linearly from the first value of the acceptor doping density up to the concentration 3.2×E17 cm^{-3} which gives the maximum value such as V_{OC}=1.16 V, FF=88.1% and PCE=33.7%, unlike the current, which decreases from top to bottom successively from J_{SC}=33.42 mA/cm^2 to 33.15 mA/cm^2. A further increase in doping concentration will lead to a higher rate of Auger recombination, which is not beneficial for cell performance. It can be noticed from Fig.6 (b) that when the doping density of the acceptor N_A exceeds 3.2×E15 cm^{-3}, we observe a rapid drop in J_{SC} as hole transport is strongly attuned because of the enhanced impurity scattering and recombination. In conclusion, we choose an acceptor doping density of 3.2×E17 cm^{-3} [34, 35].

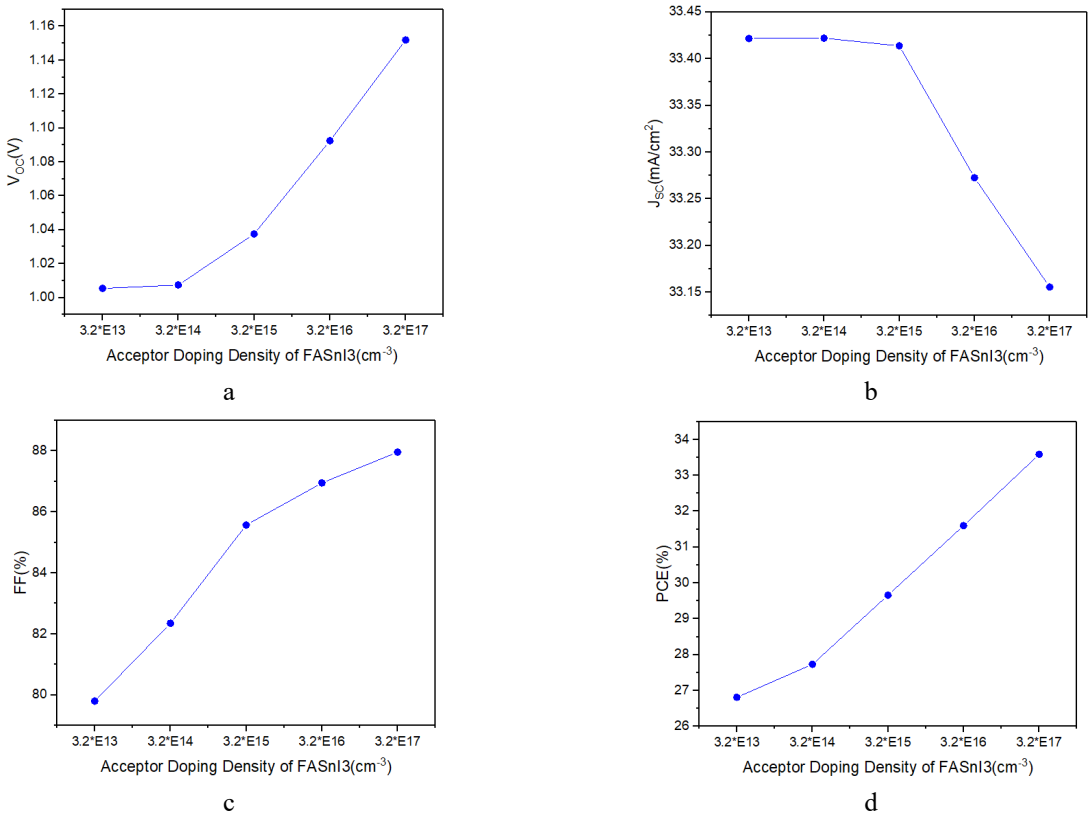

Figure 6. Variation of PV parameters as a function of acceptor doping density

4.5 The Impact of CeO_2 and PTAA doping density

The impact of doping on the charge transport layer (ETL and HTL) in a solar cell can have significant effects on various photovoltaic parameters since doping density will affect the mobility of charge carriers (electrons or holes) within the layer, improve conductivity and reduce recombination [36, 37]. Firstly, in the current section, we will study the impact of the ETL material, CeO_2, at different donor doping densities, as shown in Figure 7. For all values between E13 cm^{-3} and E20 cm^{-3}, we observe that up to a donor density of E17 cm^{-3}, parameters increase such as J_{SC}=33.388 mA/cm^2, FF=83.5%, PCE=28.95%, in contrast to V_{OC} which decreases rapidly from E17 cm^{-3}, corresponding to an open circuit voltage of 1.0396 V.

Francisco Peña-Camargo et al. explained that the doping density is only decisive for device performance when the density exceeds a certain threshold, which is of the order of E16 cm^{-3}, and that it is only above this threshold that internal electric field begins to have a positive impact on charge carriers [38]. The internal electric field then increases with the doping density, accelerating carrier transport and improving conductivity as well as the other parameters except for V_{OC}, which will decrease slightly as a result of the improved conductivity [39]. After optimization, we select the donor doping concentration of the CeO_2 in the order of E19 cm^{-3}.

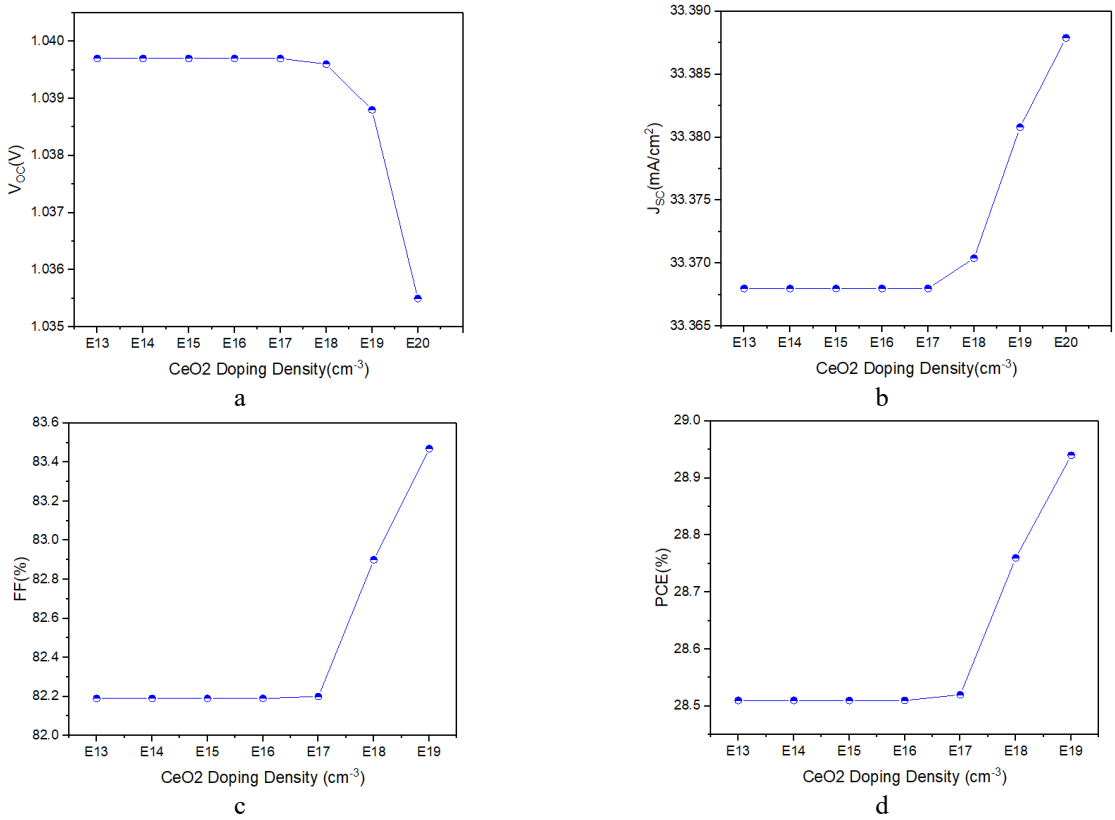

Figure 7. Variation of PV parameters as a function of CeO_2 doping density

The second part of this section examines the perovskite solar cell by optimizing the HTL material for different PTAA layer acceptor doping density values. Device performance shows a direct influence as doping increases, and the analysis was carried out by varying the acceptor doping density from 1.5×E13 cm^{-3} to 1.5×E20 cm^{-3} as shown in Figure 8.

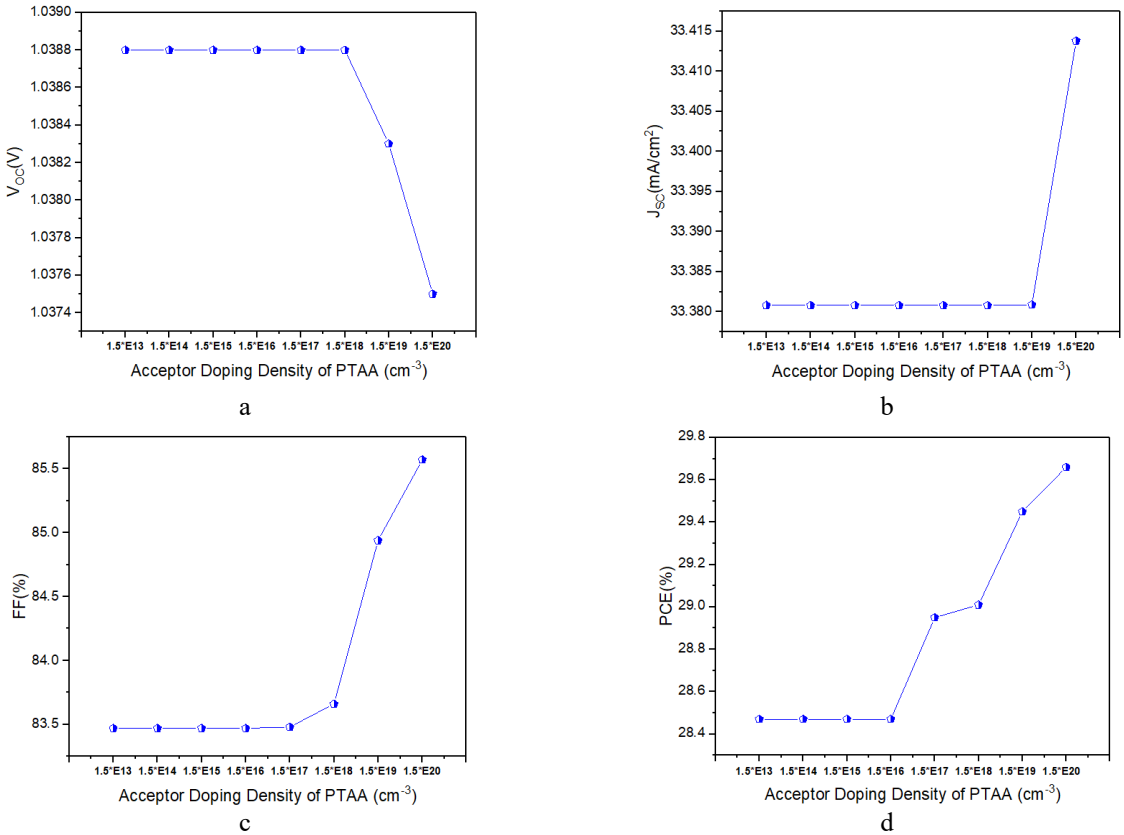

Figure 8. Variation of PV parameters as a function of PTAA doping density

This shows that device performance is slightly influenced by doping density up to E20 cm^{-3}, if we increase the doping concentration, charge carrier separation increases and cell performance also increases as follows: J_{SC}=33.41 mA/cm^2, FF=85.6%, PCE=29.7%, in contrast to the V_{OC}, which shows decreasing values from 1.0388 V to 1.0375 V as depicted in Fig.8 (a)

4.6 The Impact of defect density on the output parameters

Solar cell performance also depends on the density of defects, which are considered to be limiting factors since they affect recombination, lifetime and carrier mobility. Increasing the number of defects (N_t) results in a high rate of recombination, which in turn reduces the number of charge carriers, thereby decreasing the V_{OC}, J_{SC}, PCE and FF [40-42]. Figure 9 shows the influence of the defect density in the perovskite layer on the PSC performance.

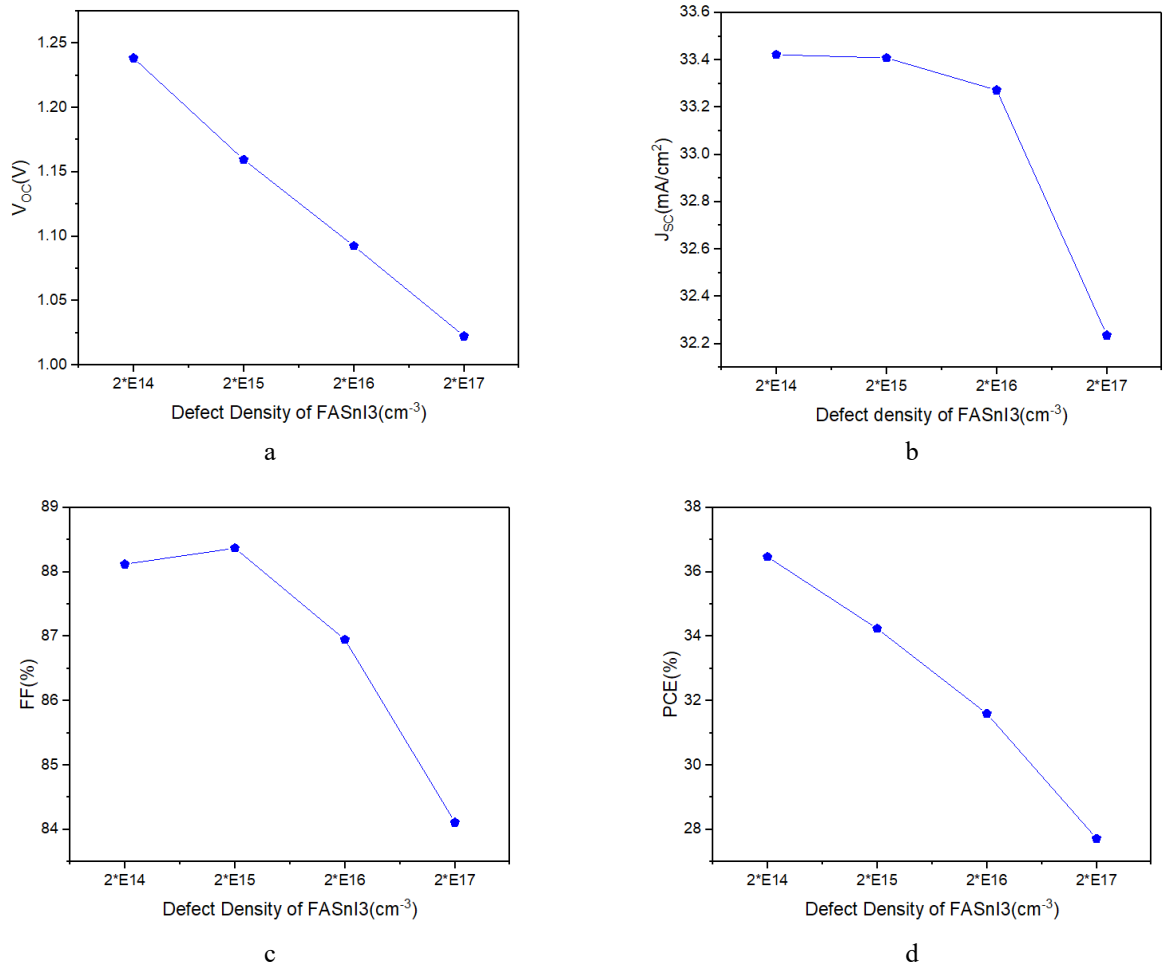

Figure 9. Variation of PV parameters as a function of the absorber layer defect density

The used defect density ranged from 2×E14 cm^{-3} to 2×E17 cm^{-3}. The output device reversely proportional with defect density, when we increase defect density the output parameters fall down as follows, J_{SC} from 33.4 mA/cm^2 to 32.2 mA/cm^2, V_{OC} from 1.24 V to 1.025 V, FF from 88.5 % to 84 % and PCE from 36.5 % to 27.6 %. Based on the optimization performed, we choose a defect density of 2×E14 cm^{-3} as the appropriate value that brings the best improvement to the photovoltaic and electrical output parameters.

4.7 The Impact of series resistances on the output parameters

The series resistance of a solar cell is due to several causes, in addition to manufacturing faults, defects and interfaces between the various materials, as well as resistances in the front and rear contacts. The main impact of series resistance is to reduce the fill factor, although excessively high values can also reduce the short-circuit current [43, 44].

The current simulation varies the series resistance value from 0 Ω.cm^2 to 8 Ω.cm^2 and optimize its adequate value of the good performance of the photovoltaic device. The Fig. 10 illustrates the output parameters of the solar cell device of, J_{SC}, V_{OC}, FF, PCE for a range of series resistance, J_{SC} decreases as series resistance increases, the V_{OC} has a value of 1.24 V from 0 Ω.cm^2 to 6 Ω.cm^2 and at 8 Ω.cm^2 the voltage increases to 1.36 V. As shown in Fig.10 (c and d), both FF and PCE decrease with increasing series resistance. The figure also shows that the FF has its good percentage of 88.2% at 0 Ω.cm^2 and that the PCE also has its optimal value of 36.5% at 0 Ω.cm^2.

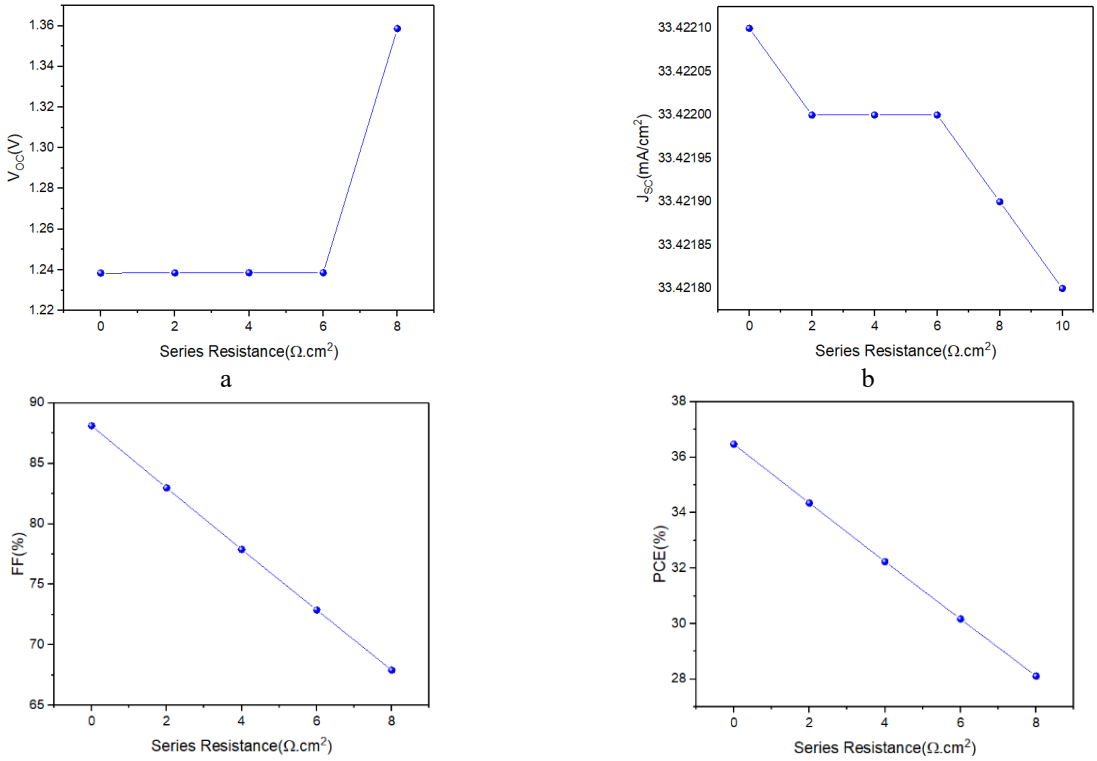

Figure 10. Variation of PV parameters as a function of series resistance

4.8 Adequate back contact for the PSC

The contact material has a major impact on the electrical performance of the solar cell, but in practice other factors such as cost and chemical and photochemical stability must also be taken into account when choosing the back contact material [45, 46]. In this section is devoted to finding the right back contact by analyzing the impact of work function on the solar cell output parameters. The examination of the device involves the use of numerous materials such as Ag, Cu, C and Au as back contact. Figure 11 below shows the solar cell's output parameters: J_{SC}, V_{OC}, FF and PCE.

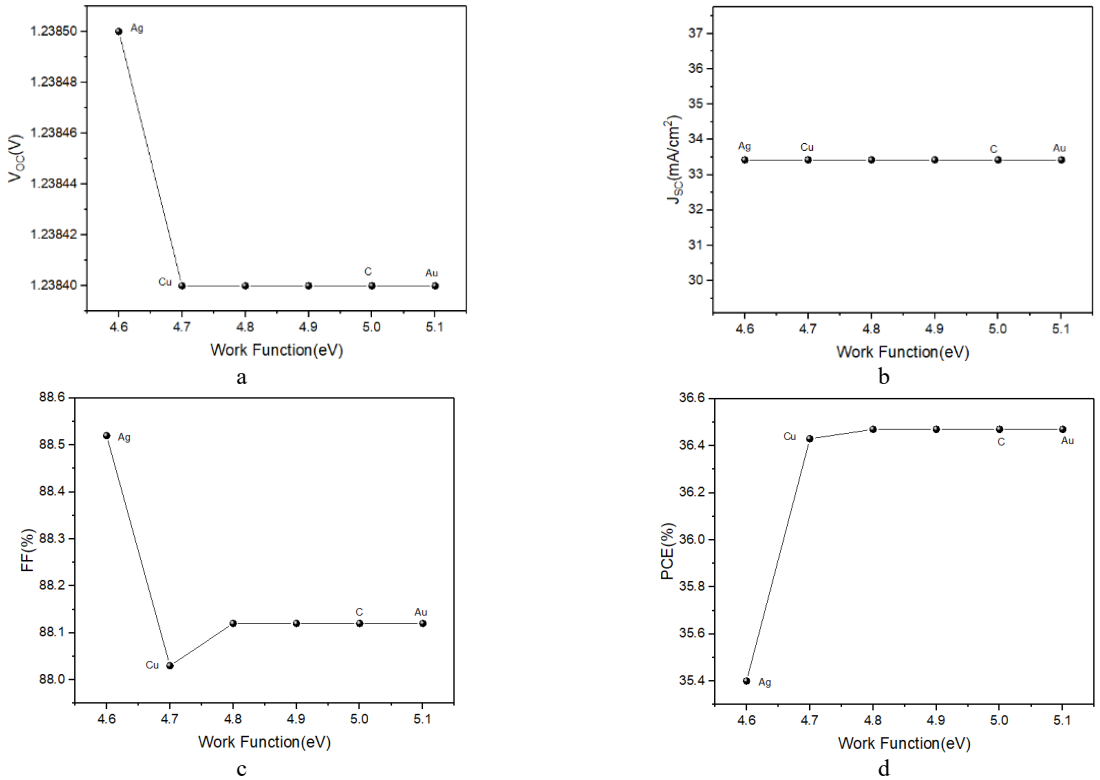

Figure 11. Impact of work function on the solar cell output parameters

The J_{SC} has a constant value of 33.4 mA/cm^2 for all materials used, the optimal V_{OC} of 1.2385 V at the Ag material, the file factor has 88.53% also for Ag while the PCE has the value of 35.4% with Ag and reaching 36.5% for the other materials. As a results of this part of the work function, the figures show that Ag is the appropriate back contact material for its good PSC performance, unfortunately it has been reported that Ag-based back contact suffers from degradation over time with the formation of silver iodide (AgI), that's why Au is the optimal choice for achieving the compromise between stability and performance.

4.9 The contour study of the FASnI3 based PSC

As shown in Fig. 12, the optimal values of the output parameters are described as follows, the current J_{SC}=33.7 mA/cm^2 for the thickness of 0.8 nm and more and for the whole range used (from E14 cm^{-3} to E18 cm^{-3}) of the $FASnI_3$ absorber doping concentration, the optimal voltage V_{OC}=1. 31 V obtained when the absorber becomes very thin starting from 0.6 nm with a higher doping concentration of E18 cm^{-3}, the high doping concentration at E18 cm^{-3} is the optimum value, corresponding to a fill factor of 90.12% for all thickness ranges used (from 0.4 nm to 1.2 nm). Finally, using the coordinates of a doping concentration of E18 cm^{-3} and a thickness value greater than or equal to 0.6 nm, we obtain a PCE peak of 39.24%.

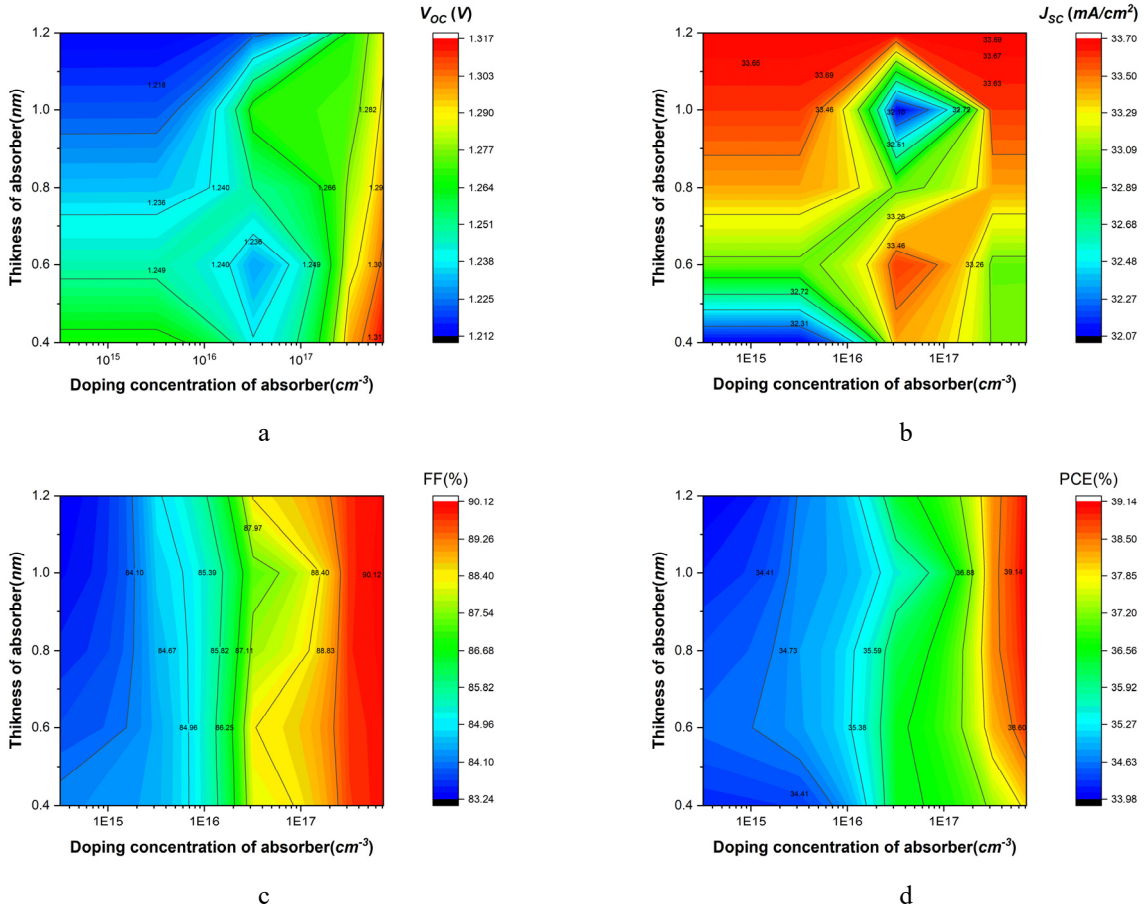

Figure 12. Impact of the absorber layer doping concentration on the PSC Output parameters (V_{OC}, J_{SC}, FF, and PCE)

CONCLUSIONS

In this article, we have numerically simulated the configuration of ITO/CeO_2/$FASnI_3$/PTAA/Au using SCAPS-1D simulation software. The absorber layer performance was optimized by adjusting defect density, acceptor density and absorber layer thickness. It was found that the optimal absorber thickness is 0.6 µm, the absorber defect density is 2×E14 cm^{-3}, while the absorber doping concentration is 3.2×E17 cm^{-3}. For the ETL and HTL layers, ideal performance was achieved with a thickness of 0.005µm for CeO_2 and 0.025 µm for PTAA. Their optimal doping concentration was found to be E19 cm^{-3}.

Finally, and after full optimization, the resulting perovskite solar cell achieves an efficiency of 39.24 % as a result from multiplying J_{SC}, V_{OC} and FF successively of 33.7 mA/cm^2, 1.31 V and 90.12 %. The results present a good enhancement of the photovoltaic and electrical output parameters making the reported configuration using $FASnI_3$ offers a viable route to achieve PSC that has no lead toxicity, as well as low cost and high efficiency.

ORCID

Abderrahim Yousfi, https://orcid.org/0000-0003-2071-728X; **Okba Saidani,** https://orcid.org/0000-0003-0507-5581

REFERENCES

[1] A.R. Mollick, and Md.A. Ashraf, "Numerical Simulation of Cs2AgBiBr6-based Perovskite Solar Cell with ZnO Nanorod and P3HT as the Charge Transport Layers," Physica B: Condensed Matter, **618**, 413187 (2021). https://doi.org/10.1016/j.physb.2021.413187

[2] A. Yousfi, O. Saidani, Z. Messai, R. Zouache, *et al*., "Design and Simulation of a Triple Absorber Layer Perovskite Solar Cell for High Conversion Efficiency," East European Journal of Physics, (4), 137-146 (2023). https://doi.org/10.26565/2312-4334-2023-4-14

[3] NREL Efficiency chart, (2023), https://www.nrel.gov/pv/assets/images/cell-pv-eff-emergingpv.png

[4] E. Zimmermann, K. Wong, M. Müller, H. Hu, P. Ehrenreich, *et al*., "Characterization of perovskite solar cells: Towards a reliable measurement protocol," APL Materials, **4**(9), 091901 (2016). https://doi.org/10.1063/1.4960759

[5] O.A. Muhammed, E. Danladi, P.H. Boduku, J. Tasiu, M.S. Ahmad, and N. Usman, "Modeling and Simulation of Lead-Free Perovskite Solar Cell Using SCAPS-1D," East European Journal of Physics, (2), 146-154 (2021). https://doi.org/10.26565/2312-4334-2021-2-12

[6] C.H. Liao, Md.A. Mahmud, and A. Ho-Baillie, "Recent progress in layered metal halide perovskites for solar cells, photodetectors, and field-effect transistors," Nanoscale, **15**, 4219-4235 (2023). https://doi.org/10.1039/D2NR06496K

[7] E. Danladi, D.S. Dogo, S.U. Michael, F.O. Uloko, and A.O. Salawu, "Recent Advances in Modeling of Perovskite Solar Cells Using SCAPS-1D: Effect of Absorber and ETM Thickness," East European Journal of Physics, (4), 5-17 (2021). https://doi.org/10.26565/2312-4334-2021-4-01

[8] S. Rabhi, H. Benzouid, A. Slami, and K. Dadda, "Modeling and Numerical Simulation of a CH3NH3SnI3 Perovskite Solar Cell Using the SCAPS1-D Simulator," Eng. Proc. **56**(1), 97 (2023). https://doi.org/10.3390/ASEC2023-15300

[9] S. Imani, S.M. Seyed-Talebi, J. Beheshtian, *et al*., "Simulation and characterization of CH3NH3SnI3-based perovskite solar cells with different Cu-based hole transporting layers," Appl. Phys. A, **129**, 143 (2023). https://doi.org/10.1007/s00339-023-06428-0

[10] L. Ghalmi, S. Bensmaine, and C.E.H. Merzouk, "Optimizing the Performance of Lead-free CH3NH3SnI3 Perovskite Solar Cells via Thickness, Doping, and Defect Density Control," Journal of Science, Technology and Engineering Research, **4**(1), 44-51 (2023). https://doi.org/10.53525/jster.1231984

[11] M.K. Hossain, M. Rubel, G.F.I. Toki, *et al*., "Effect of Various Electron and Hole Transport Layers on the Performance of CsPbI3-Based Perovskite Solar Cells: A Numerical Investigation in DFT, SCAPS-1D, and wxAMPS Frameworks," ACS Omega, **7**, 43210−43230 (2022). https://doi.org/10.1021/acsomega.2c05912

[12] E. Katunge, G. Njema, and J. Kibet, "Theoretical analysis of the electrical characteristics of lead-free formamidinium tin iodide solar cell," IET Optoelectronics, **17**(5), 220-236 (2023). https://doi.org/10.1049/ote2.12104

[13] P. Tiwari, M.F. Alotaibi, Y. Al-Hadeethi, V. Srivastava, *et al*., "Design and Simulation of Efficient SnS-Based Solar Cell Using Spiro-OMeTAD as Hole Transport Layer," Nanomaterials, **12**(14), 2506 (2022). https://doi.org/10.3390/nano12142506

[14] A.B. Coulibaly, S.O. Oyedele, N.R. Kre, and B. Aka, "Comparative Study of Lead-Free Perovskite Solar Cells Using Different Hole Transporter Materials. Modeling and Numerical Simulation," Modeling and Numerical Simulation of Material Science, **9**(4), 97-107 (2019). https://doi.org/10.4236/mnsms.2019.94006

[15] A.K. Al-Mousoi, M.K.A. Mohammed, R. Pandey, J. Madan, *et al*., "Simulation and analysis of lead-free perovskite solar cells incorporating cerium oxide as electron transporting layer," RSC Adv. **50**(12), 32365-32373 (2022). https://doi.org/10.1039/D2RA05957F

[16] K. Ukoba, P.E. Imoisili, and T.C. Jen, "Numerical analysis and performance improvement of nanostructured Cu2O/TiO2pn heterojunction solar cells using SCAPS," Materials Today: Proceedings, **38**(2), 887-892 (2021). https://doi.org/10.1016/j.matpr.2020.05.111

[17] M. Burgelman, P. Nollet, and S. Degrave, "Modelling polycrystalline semiconductor solar cells," Thin Solid Films, **361–362**, 527-532 (2000). https://doi.org/10.1016/S0040-6090(99)00825-1

[18] S. Bhattarai, D. Borah, J. Rout, R. Pandey, J. Madan, *et al*., "Designing an efficient lead-free perovskite solar cell with green-synthesized $CuCrO_2$ and CeO_2 as carrier transport materials," RSC Adv. **13**(49), 34693-34702 (2023). http://dx.doi.org/10.1039/D3RA06722J

[19] Sk.T. Ahamed, Ar. Basak, A. Mondal, "Device modeling and investigation of Sb-based low-cost heterojunction solar cells using SCAPS-1D," Results in Optics, **10**, 100364 (2023). https://doi.org/10.1016/j.rio.2023.100364

[20] M. Ismail, M. Noman, S.T. Jan, and M. Imran, "Boosting efficiency of ecofriendly perovskite solar cell through optimization of novel charge transport layers," R. Soc. Open Sci. **10**(6), 230331 (2023). https://doi.org/10.1098/rsos.230331

[21] S.T. Jan, and N. Muhammad, "Influence of layer thickness, defect density, doping concentration, interface defects, work function, working temperature and reflecting coating on lead-free perovskite solar cell," Solar Energy, **237**, 29-43 (2022). https://doi.org/10.1016/j.solener.2022.03.069

[22] B. Atanu, R. Radhakrishnan, R. Nekovei, and R. Jeyakumar, "Effect of absorber layer, hole transport layer thicknesses, and its doping density on the performance of perovskite solar cells by device simulation," Solar Energy, **196**, 177-182 (2020). https://doi.org/10.1016/j.solener.2019.12.014

[23] I. Mesquita, L. Andrade, and A. Mendes, "Temperature Impact on Perovskite Solar Cells Under Operation," Chem. Sus. Chem. **12**(10), 2186-2194 (2019). https://doi.org/10.1002/cssc.201802899

[24] P. Roy, N.K. Sinha, and A. Khare, "An investigation on the impact of temperature variation over the performance of tin-based perovskite solar cell: A numerical simulation approach," Materials Today: Proceedings, **39**(5), 2022-2026 (2021). https://doi.org/10.1016/j.matpr.2020.09.281

[25] H. Baig, H. Kanda, A.M. Asiri, M.K. Nazeeruddin, and T. Mallick, "Increasing efficiency of perovskite solar cells using low concentrating photovoltaic systems," Sustainable Energy Fuels, **4**(2), 528-537 (2020). http://dx.doi.org/10.1039/C9SE00550A

[26] A. Gholami-Milani, S. Ahmadi-Kandjani, B. Olyaeefar, *et al*., "Performance analyses of highly efficient inverted all-perovskite bilayer solar cell," Sci. Rep. **13**, 8274 (2023). https://doi.org/10.1038/s41598-023-35504-x

[27] R. Priyanka, T. Sanjay, and K. Ayush, "An investigation on the influence of temperature variation on the performance of tin (Sn) based perovskite solar cells using various transport layers and absorber layers," Results in Optics, **4**, 100083, (2021). https://doi.org/10.1016/j.rio.2021.100083

[28] N. Rono, A.E. Merad, J.K. Kibet, *et al*., "A theoretical investigation of the effect of the hole and electron transport materials on the performance of a lead-free perovskite solar cell based on $CH_3NH_3SnI_3$," J. Comput. Electron. **20**, 993–1005 (2021). https://doi.org/10.1007/s10825-021-01673-z
[29] J. Arayro, R. Mezher, and H. Sabbah, "Comparative Simulation Study of the Performance of Conventional and Inverted Hybrid Tin-Based Perovskite Solar Cells," Coatings, **13**(7), 1258 (2023). https://doi.org/10.3390/coatings13071258
[30] O. Mostafa, N.A. Zidan, W. Abbas, H.H. Issa, N. Gamal, and M. Fedawy, "Design and performance optimization of lead-free perovskite solar cells with enhanced efficiency," Mathematical Modelling of Engineering Problems, **10**(4), 1307-1316 (2023). https://doi.org/10.18280/mmep.100424
[31] G.W. Kim, D. Shinde, and T. Park, "Thickness of the hole transport layer in perovskite solar cells: performance versus reproducibility," RSC Adv. **5**(120), 99356-99360 (2015). http://dx.doi.org/10.1039/C5RA18648J
[32] Md.A. Islam, Md.N.B. Alamgir, S.I. Chowdhury, and S.M.B. Billah, "Lead-free organic inorganic halide perovskite solar cell with over 30% efficiency," Journal of Ovonic Research, **18**, 395-409 (2022). https://doi.org/10.15251/JOR.2022.183.395
[33] H. Sabbah, J. Arayro, and R. Mezher, "Simulation and Investigation of 26% Efficient and Robust Inverted Planar Perovskite Solar Cells Based on $GA_{0.2}FA_{0.78}SnI_3$-1%EDAI2 Films," Nanomaterials, **12**, 3885 (2022). https://doi.org/10.3390/nano12213885
[34] Hui-Jing Du, *et al*., "Device simulation of lead-free CH3NH3SnI3 perovskite solar cells with high efficiency," Chinese Physics B, **25**(10), 108802 (2016). https://dx.doi.org/10.1088/1674-1056/25/10/108802
[35] P.K. Patel, "Device simulation of highly efficient eco-friendly $CH_3NH_3SnI_3$ perovskite solar cell," Sci. Rep. **11**, 3082 (2021). https://doi.org/10.1038/s41598-021-82817-w
[36] V.M. le Corre, M. Stolterfoht, L.P. Toro, M. Feuerstein, *et al*., "Charge Transport Layers Limiting the Efficiency of Perovskite Solar Cells: How to Optimize Conductivity, Doping, and Thickness," ACS Appl. Energy Mater. **2**, 6280−6287 (2019). https://doi.org/10.1021/acsaem.9b00856
[37] J. Avila, L. Gil-Escrig, P. Boix, M. Sessolo, S. Albrecht, and H.J. Bolink, "Influence of doped charge transport layers on efficient perovskite solar cells," Sustainable Energy Fuels, **2**(11), 2429-2434 (2018). http://dx.doi.org/10.1039/C8SE00218E
[38] F. Peña-Camargo, J. Thiesbrummel, H. Hempel, A. Musiienko, *et al*., "Revealing the doping density in perovskite solar cells and its impact on device performance," Appl. Phys. Rev. **9**(2), 021409 (2022). https://doi.org/10.1063/5.0085286
[39] M. Ahamad, and A.K.M. Hossain, "Design and optimization of non-toxic and highly efficient tin-based organic perovskite solar cells by device simulation," Heliyon, **9**(9), e19389 (2023). https://doi.org/10.1016/j.heliyon.2023.e19389
[40] Y. Wan-Jian, S. Tingting, and Y. Yanfa, "Unusual defect physics in CH3NH3PbI3 perovskite solar cell absorber," Appl. Phys. Lett. **104**(6), 063903 (2014). https://doi.org/10.1063/1.4864778
[41] S.H. Huang, Z. Rui, D. Chi, and D. Bao, "Influence of defect states on the performances of planar tin halide perovskite solar cells," J. Semicond. **40**(3), 032201 (2019). http://doi.org/10.1088/1674-4926/40/3/032201
[42] H.K. Ibrahim, A.M.A. Sabaawi, and Q.T. Aljwari, "A Comprehensive Study on the Effect of Defects on Perovskite Solar Cell Performance," Preprints, **1**, 344 (2023). https://doi.org/10.20944/preprints202306.0344.v1
[43] S.R. Hosseini, M. Bahramgour, P.Y. Sefidi, *et al*., "Investigating the effect of non-ideal conditions on the performance of a planar," Heliyon, **8**(11), e11471 (2022). https://doi.org/10.1016/j.heliyon.2022.e11471
[44] R. Ranjan, N. Anand, M.N. Tripathi, *et al*., "SCAPS study on the effect of various hole transport layer on highly efficient 31.86% eco-friendly CZTS based solar cell," Sci. Rep. **13**, 18411 (2023). https://doi.org/10.1038/s41598-023-44845-6
[45] F. Behrouznejad, S. Shahbazi, N. Taghavinia, *et al*., "A study on utilizing different metals as the back contact of CH3NH3PbI3 perovskite solar cells," J. Mater. Chem. A, **4**(35), 13488–13498 (2016). https://doi.org/10.1039/C6TA05938D
[46] H. Sharma, and R. Srivastava, "Solution-processed pristine metal oxides as electron-transporting materials for perovskite solar cells," Front. Electron. Mater. **3**, 1174159 (2023). https://doi.org/10.3389/femat.2023.1174159

ПІДВИЩЕННЯ ПРОДУКТИВНОСТІ СОНЯЧНИХ ПЕРОВСКІТНИХ ЕЛЕМЕНТІВ FASnI3 ШЛЯХОМ ЧИСЕЛЬНОГО МОДЕЛЮВАННЯ ТА ОПТИМІЗАЦІЇ

Лахсен Кануні[a], Ламір Саїді[a], Абдеррахім Юсфі[b], Окба Сайдані[b]
[a]Лабораторія вдосконаленої автоматизації та системного аналізу (LAAAS), Департамент електроніки, Університет Батна 2, Батна 05000, Алжир
[b]Лабораторія ETA, Департамент електроніки, Факультет науки і технологій, Університет Мохамеда Ель Бачіра Ель Ібрагімі, Бордж Бу Арреріджж-34030, Алжир

Сонячні елементи на основі перовскіту в даний час привертають все більший інтерес дослідників і промисловості завдяки перевагам цього типу сонячних елементів, зокрема з точки зору простоти виробництва та багатообіцяючої ефективності перетворення електроенергії, яка нещодавно досягла надзвичайного рівня. Ця стаття зосереджена на чисельному моделюванні для покращення продуктивності конфігурації сонячної батареї на основі йодиду формамідинію олова ($FASnI_3$) за допомогою використання діоксиду церію (CeO_2) як ETL та полі (триариламіну) (PTAA) як HTL. Моделювання було виконано за допомогою інструменту Solar Cell Capacitance Simulator (SCAPS-1D) у спектрі AM 1.5 G. Було реалізовано інтенсивне моделювання для покращення вихідних параметрів запропонованої конфігурації на основі $FASnI_3$ як поглинача. Запропонована структура (ITO/CeO_2/$FaSnI_3$/PTAA/Au) забезпечує велику ефективність перетворення потужності (PCE) 39,24%, напругу холостого ходу (VOC) 1,31 В, щільність струму короткого замикання (JSC) 33,7 мА/см^2 і коефіцієнтом заповнення (FF) 90,12%.

Ключові слова: *сонячний елемент; $FASnI_3$; SCAPS-1D; оптимізація; PCE*